Integrated aerodynamic and structural blade shape optimisation of axial turbines operating with supercritical carbon dioxide blended with dopants

Abdelrahman S. Abdeldayem[1], Martin T. White[1], Andrea Paggini[2], Marco Ruggiero[2], Abdulnaser I. Sayma[1]

[1] Thermo-Fluids Research Centre, School of Mathematics, Computer science and Engineering,

City, University of London. EC1V 0HB, United Kingdom

[2] Turbomachinery & Process Solutions, Baker Hughes, Via Felice Matteucci, Firenze, 50127, Italy

Corresponding author: abdel-rahman.abdeldayem@city.ac.uk

ABSTRACT

Within this study, the blade shape of a large-scale axial turbine operating with sCO_2 blended with dopants is optimised using an integrated aerodynamic-structural 3D numerical model, whereby the optimisation aims at maximising the aerodynamic efficiency whilst meeting a set of stress constraints to ensure safe operation. Specifically, three candidate mixtures are considered, namely CO_2 blended with titaniumtetrachloride ($TiCl_4$), hexafluorobenzene (C_6F_6) or sulfur dioxide (SO_2), where the selected blends and boundary conditions are defined by the EU project, SCARABEUS. A single passage axial turbine numerical model is setup and applied to the first stage of a large-scale multi-stage axial turbine design. The aerodynamic performance is simulated using a 3D steady-state viscous computational fluid dynamic (CFD) model while the blade stress distribution is obtained from a static structural finite element analysis (FEA). A genetic algorithm is used to optimise parameters defining the blade angle and thickness distributions along the chord line while a surrogate model is used to provide fast and reliable model predictions during optimisation using genetic aggregation response surface. The uncertainty of the surrogate model represented by the difference between the surrogate model results and the CFD/FEA model results is evaluated using a set of verification points and found to be less than 0.3% for aerodynamic efficiency and 1% for both the mass flow rate and the maximum equivalent stresses. The comparison between the final optimised blade cross-sections have shown some common trends in optimising the blade design by decreasing stator and rotor trailing edge thickness, increasing stator thickness near the trailing edge, decreasing rotor thickness near the trailing edge and decreasing the rotor outlet angle. Further investigations of the loss breakdown of the optimised and reference blade

designs are presented to highlight the role of the optimisation process in reducing aerodynamic losses. It has been noted that the performance improvement achieved through shape optimisation is mainly due to decreasing the endwall losses of both stator and rotor blades.

Keywords: Axial Turbines, Blade-shape optimisation, Supercritical Carbon Dioxide, sCO_2, sCO_2 Blends.

1 INTRODUCTION

Introducing new working fluids like supercritical carbon dioxide (sCO2) and sCO2 blended with dopants in power generation cycles has a high potential to increase the thermal efficiency and decrease the associated capital and operational costs [1, 2]. Numerous studies have focused on analysing the performance of pure sCO2 power plants as well as sCO2 mixtures [3] where the results have proven that introducing blends to the cycle potentially increase the efficiency and ensure feasible operation of transcritical power cycles especially in hot weather. As part of the EU project, SCARABEUS, three candidate blends namely titaniumtetrachloride (TiCl4), hexafluorobenzene (C6F6) and sulfur dioxide (SO2), have been proposed to raise the critical temperature of the mixture beyond that of pure CO2 and allow condensation in transcritical power cycles. Crespi et al. [4] investigated the power cycle thermal efficiency gain by blending carbon dioxide with C6F6 and TiCl4. The results of cycle analyses have shown that sCO2 blends, with blend molar fractions of 10-25%, have thermal efficiency gains of 4-5 percentage points over the pure sCO2 cycle due to the deleterious effect of high ambient temperatures on the compression process in the latter cycles. The use of CO2 blended with SO2 has also been considered through an economic and thermodynamic assessment which revealed an increase in cycle thermal efficiency of 2.33% relative to the pure sCO2 cycle and a reduction of the power block capital expenses of 160 $/kWel for a 100MWel power cycle [5].

The turbomachinery components operating with sCO_2 and sCO_2 mixtures have been previously introduced [6, 7]. The performance of different blends and the effect of blend fraction has also been recently investigated [8] with much focus on predicting the thermodynamic properties of mixtures, including the selection of equation of state and the optimum binary interaction parameters [9].

The design process of turbines operating with sCO_2 mixtures introduces some technical challenges related to the availability of loss models used for preliminary design. Specifically, the available performance estimation tools and correlations are calibrated for traditional working fluids like steam and air, whilst novel methodologies are required to simulate newly developed working fluids [10]. The design process of a turbine first requires a mean-line

flow path design, from which a 1D geometry is generated that can be used as the base to create the 3D blade and run computational fluid dynamics simulations (CFD). Blade shape optimisation is then one of the promising techniques to optimise the turbine design by refining the flow path geometry to obtain the highest possible aerodynamic performance while maintaining certain structural limits to ensure a safe and reliable design.

Blade shape optimisation has been widely investigated throughout the literature using different approaches, tools, and methodologies. Sathish *et al.* [11] conducted a blade shape optimisation of a 10 MW sCO_2 axial turbine stage aiming at minimising the blade profile losses while maintaining certain limits to the geometry. The selected geometric modelling platform was CAESES® while the numerical flow solver was MISES. Many authors have used the commercial flow solver ANSYS CFX to simulate the aerodynamic performance in their optimisation models [12-16] while the optimisation solver is commonly genetic algorithm (GA) and multi-objective genetic algorithm (MOGA) [17-19]. Various optimisation objectives have been presented through the published studies, however the common target is achieving higher aerodynamic performance. Berchiolli *et al.* [13], Klonowicz *et al.* [14], Asgarshamsi *et al.* [17] and Kawatsu *et al.* [19] have defined the optimisation objectives to explicitly to maximise the overall turbine efficiency while Cho *et al.* [20] and Ennil *et al.* [16] have minimised the total pressure loss coefficient.

Decision variables selected for the blade shape optimisation models are usually linked to geometrical parameters defining the aerofoil shape in 2D models [18] and 3D angles in 3D model [14]. The geometrical representation of the blade is critical to defining the number of decision variables that need to be included. Ennil *et al.* [16] introduced 11 parameters including flow angles, axial blade chord, turning angle, leading edge radius and trailing edge thickness to represent the aerofoil shape of the blade. Similar approach is followed by [20], in which the authors defined the blade using 13 parameters. In more sophisticate studies, a larger number of variables are used to parametrise the pressure and suction sides of the blade using control point coordinates. Berchiolli *et al.* [13] introduced 48 decision variables and Klonowicz *et al.* [14] introduced 50 decision variables in their model including 3D aspects such as rotor blade twist angle, circumferential lean and axial sweep angles. In some specific applications, decision variables are limited to certain parameters that define a part of the blade to minimise a specific source of loss; e.g. optimising the blade tip to minimise tip leakage characteristics [12].

Due to the large number of decision variables required to represent a complete blade shape, a common optimisation approach is based on replacing the physical CFD model with a surrogate model to give faster response

during optimisation process. Surrogate models are created using a number of physical CFD simulations while the model response is extended by creating a relation between inputs and outputs using machine learning techniques. A set of case studies are firstly designed using a design of experiments algorithm (DoE) that creates a map of trial cases from which a relation between the inputs and outputs can be constructed. The response surface is then created using one of various techniques including Kriging [19], artificial neural network (ANN) [12, 21], extreme learning machine (ELM) and support vector machine (SVM) [12].

The optimisation constraints are introduced to the model to verify the feasibility of the different candidate designs generated using combinations of decision variables. Berchiolli *et al.* [13] constrained the power output, the global maximum Mach number and the stator and rotor factor of safety (FOS) while other studies were only concerned with geometric constraints to ensure that the optimised profile meets all engineering constraints [11, 20]. The structural analysis is important to ensure a safe blade design and have been introduced in many studies [22, 23], although with added complexity to the model. Common materials in structural simulations of axial turbines are Inconel 718 [22], Inconel 738 [13] and 12% Chromium steel [11]. The loading in structural analysis is defined using either mechanical loading due to aerodynamic pressure distribution [22] or thermal loading due to temperature distribution, especially for cooled blades [23].

The performance of the reference and optimised blades can be further investigated by obtaining the loss breakdown structure using one of the loss audit techniques published in the literature [24-26]. The loss audit helps to highlight the dominant sources of aerodynamic losses, so that the most significant improvements are revealed. Common types of aerodynamic losses in a subsonic axial turbine stage operating under design conditions are endwall, profile, trailing edge, and tip clearance losses.

In this paper, three working fluids have been considered for the design of a large-scale multi-stage axial flow turbine, namely CO_2 blended with titaniumtetrachloride ($TiCl_4$), hexafluorobenzene (C_6F_6) or sulfur dioxide (SO_2). The design process is based on numerical simulations rather than using existing mean-line design correlations since the latter are not calibrated for these working fluids. The design is further refined using a blade shape optimisation model that aims at maximising the performance of the turbine given certain structural constraints. A comparison between the reference and optimised blades profiles is presented and discussed to reveal different design aspects associated with different sCO_2 blends. The loss breakdown is illustrated for different working fluids compared to the reference design to show the link between turbine efficiency and different sources of aerodynamic loss.

2 NUMERICAL MODEL

The blade shape optimisation process is reported in Figure 1 and is constructed from a numerical model composed of an aerodynamic solver (CFD), a mechanical solver (FEA), a design of experiments (DoE) algorithm, a surrogate model, and an optimisation solver. The baseline blade geometry is created using a mean-line design model [27] that is developed for the SCARABEUS project [28] to design a large-scale blended sCO_2 turbine using Aungier [29] loss model. Geometrical parameters including the number of stages, hub diameter, blade height, blade inlet/outlet angles, stagger angle, chord length, number of blades and trailing edge (TE) thickness are used to create the 3D blade along with assumptions defining the inlet/outlet wedge angles, leading edge (LE) thickness and control points defining thickness distribution of the aerofoil. In order to assess the blades stresses, simplified shroud and hub geometries are attached to the stator and rotor blade geometries, respectively, to account for the fillet at each blade base of fixation and make the mechanical analysis more realistic. The results of aerodynamic solver are transferred back to the mechanical solver so that the pressure load on the blade surface is evaluated. A set of design points are then created using the DoE algorithm and solved to create a response surface surrogate model which replaces the actual CFD/FEA model to simplify the optimisation process and allow for more optimisation runs in a reasonable time frame.

2.1 CFD model

To investigate and compare the effect of different sCO_2 blends on the blade shape design and further investigate the performance of the optimised blades against the reference designs, a 3D steady-state CFD model of the first stage of each blend design is setup. Although the proposed turbine designs are for multi-stage turbines, the CFD model is setup for the first stage of each design to minimise the number of decision variable for optimisation and limit the computational power needed for this study to a reasonable time frame. Similar flow conditions defined by equal enthalpy drop per stage, equal rotational speed, and equal hub diameter are preserved for each case to ensure a fair comparison between the different blends. To achieve that, the number of stages for each blend is adjusted to give almost the same enthalpy drop per stage, thus the velocity triangles of the first stage of the three turbines, according to the mean-line calculations, are identical.

The operating conditions for the proposed case studies are part of the work delivered to the SCARABEUS project [28] where the cycle analysis generates the boundary conditions at the inlet and outlet as well as the optimum blend molar fraction. The model definition of each turbine is further investigated using a mean-line design tool

developed based on Aungier loss model [29] to generate a preliminary design of the turbines. The model definition of the proposed blends is presented in

List of tables

Table 1. The model uses shear stress transport (k-ω SST) turbulence model as it has been found that this is the most suitable model for turbomachinery applications [30]. The interface between the stator and rotor domains is treated as a mixing plane which has proven to give high quality results with the least numerical instabilities compared to the frozen rotor approach [31]. The rotor layout is considered to be unshrouded with a tip clearance of 0.07% of the tip diameter for each case.

The mesh quality has been controlled by adjusting the mesh size near the walls maintaining $y^+ \approx 50$ where standard wall functions are best suited [32]. The number of grid points within the rest of the domain is obtained as the minimum number of grid points required for a mesh independent solution. The convergence criteria of the mesh study have been selected as the total-to-total efficiency (η_{tt}) where the tolerance is set to 0.5 % compared to the finest mesh. The mesh independence study results are presented in Figure 2 for the sCO_2-C_6F_6 case study as a sample case, where the number of grid points reported is the summation of stator and rotor domains.

The thermo-physical properties of the sCO_2 mixtures are evaluated using "SIMULIS" software. The selected equation of state (EoS) is Peng Robinson, and the binary interaction parameters for each blend are set according to a sensitivity study carried out by our project partners [5, 9]. These parameters are the same as the values defined in the cycle analysis and mean-line design stages. However, it is worth noting that the mixture modelling is most critical when modelling the thermodynamic cycle, and there is not a large sensitivity when considering the turbine in isolation because the turbine operates quite far from the critical point of the fluid where non-ideal effects are most significant [9].

The properties are introduced to the CFD models using look-up tables that cover the expected pressure and temperature ranges with the size of 500×500 points. The selected pressure range is set to 10 and 300 bar since the turbine inlet total pressures are 250 bar and the outlet static pressure varies between 56 and 97 bar. This range covers any local regions with pressures higher than the inlet pressure or lower than the outlet pressures. Similarly, the temperature range is set between 400 and 1200 K. The CFD model results have been checked to ensure that the property tables can safely cover the global minimum and maximum properties where the tables limits are found to be sufficiently far away from the obtained limits. Different sizes of the lookup tables have been tested ranging between 200×200 and 700×700 points while the variations in the model results are found to be negligibly small above 500×500.

2.2 FEA model

The finite element analysis (FEA) model is setup using the same blade geometry defined for the CFD model. However, the blade geometry is modified by adding a solid base with a minimum thickness of 5 mm at the shroud of the stator and at the hub for the rotor with fillets applied between the blade and the supporting base to represent the physical turbine geometry after manufacturing. Adding the fillets also avoids numerically induced peak stresses, as indicated in Figure 3.

The mesh size in this model is designed with a large global element size to simplify the optimisation process and reduce the overall model complexity while local fine elements are defined at the base fillet where the peak stress point is expected to exist. With a growth rate of 1.1, which defines the ratio between the large elements at the tip and the small elements at the base, the overall mesh structure produces satisfactory results for a low number of elements. A mesh study is summarised in Figure 4 where the different curves represent the global element size, and the callouts report the local element size at the base of the fillet in mm. It can be noted from the figure that decreasing the global mesh size affects the total number of nodes significantly while its effect on the stress values is negligible. However, the local mesh size has a large impact on the peak stresses. For that reason, a large global size of 3 mm is selected along with a local mesh size of 0.3 mm to achieve results of a satisfactory quality with a low number of nodes. The stress results in this case showed a deviation within 2% of the most accurate value where the number of elements is around 90k and 120k for the stator and rotor blades, respectively.

The aerodynamic loads (i.e., pressure distribution over the blade surfaces) predicted within the CFD simulations are used as input boundary conditions for the FEA, along with the centrifugal load on the rotor blades due to rotation. The preliminary material selection process has considered Udimet 720, which is a nickel based alloy commonly used with gas turbine blades that can operate at temperatures up to 1000 ^{o}C whilst maintaining a high yield strength suitable for the proposed operating conditions [33].

2.3 Surrogate model

The surrogate model replaces the physical CFD/FEA model so that the objectives and constraints can be assessed rapidly. This can be achieved by building a relation between input geometrical parameters and output aerodynamic and structural performance parameters using machine learning techniques. In this study, the central composite design of experiment algorithm is used to create a set of learning points according to a pre-specified range for each input optimisation variable [34]. In this method, the design points are selected to form the shape of a

sphere with a centre point in the middle surrounded by points on the axis and diagonal points; this process for two variables would create the shape in Figure 5, [35].

The number of design points (N_{DP}) is linked to the number of input variables through equation 1:

$$N_{DP} = 1 + 2k + 2^{(k-f)} \quad (1)$$

where k is the number of input variables and f is a factor designed to limit the excessive increase in the number of design points for a large number of input variables. In Equation 1, the first term is the centre of the design points, the second term represents the points on the axis and the third term represents the diagonal points. The limiting factor is added to the diagonal points to decrease the number of diagonal points while maintaining the shape of the central composite design. The factor used by the solver (ANSYS workbench) for 11 input variables is 4 so that the number of design points is 151. The disadvantage this methodology is the uncertainty in the input/output relation. However, this can be assessed and improved using response surface verification and additional refinement points respectively.

Genetic aggregation response surface (GARS) is selected for this study to develop the surrogate model as GARS with auto-refinement gives the best fit possible for each output parameter among the different types of response surface available (Full 2nd order Polynomial, Non-Parametric Regression, Kriging, Neural network and Spars grid) [36]. Compared to classical response Polynomial, Non-Parametric Regression, or Kriging Genetic Aggregation, Genetic aggregation takes more time because it solves the response surface for each output variable individually and the cross-validation process [37]. The initial number of learning points are generated using the design of experiments model while a set of refinement points are created to improve the accuracy of the response surface. The target uncertainty in total-to-total efficiency is selected to be ±0.1 pp and maximum equivalent stress is ±5 MPa. The response surface results are verified against the results of the physical CFD/FEA model for a set of verification points to assess the uncertainty of the surrogate.

2.4 Optimisation model

To obtain the best blade shape, the optimisation model is setup based on a set of geometrical parameters defining the blade shape while objectives and constraints are introduced to maintain efficient operation and a safe design. The blade geometry is represented by a uniform aerofoil section along the blade radial direction because the blades are relatively short where the blade height to hub diameter is around 8%. The angle and thickness distributions along the chord line of the aerofoil are defined from leading edge to trailing edge with four points on

each curve, as reported in Figure 7. The points are connected using a 3rd order polynomial rather than Bezier curves since polynomials give more control of the curvature with a low number of points. As long as the axial location of the first and last points are fixed at the LE and the TE, respectively, the number of variables is six variables for each curve and 24 variables for the entire stage. However, based on trials assessing the sensitivity of the results to the number of decision variables, it has been found that achieving the desired uncertainty of the output parameters is not possible using reasonable computational power, and thus the surrogate model is unable to accurately represent the physical model. This is due to the large population size and the limited number of learning and refinement points. Moreover, it was found that solving more refinement points did not allow any significant improvement in the model's accuracy. Thus, to create a surrogate model within accepted outputs tolerance, a decision was made to reduce the number of decision variables. This was done by eliminating the less dominant variables.

The procedures followed to reduce the number of decision variables can be summarised in three steps. Firstly, the streamwise division of the points are fixed for each curve so the x-values of the two mid-points are removed, and each curve now has four variables instead of six with a total number of variables of 16. Secondly, the inlet angle of the stator blade is considered fixed as the inlet flow velocity to the stage is always axial, which removes an additional variable. Finally, a preliminary sensitivity study has been conducted by creating a surrogate model using the 15 variables, as reported in Figure 6. In this figure, Sa2 is the stator angle at point 2, Sa3 is the stator angle at point 3, Sa4 is the stator angle at point 4, St1 is the stator thickness at point 1, St2 is the stator thickness at point 2, St3 is the stator thickness at point 3, St4 is the stator thickness at point 4, Ra1 is the rotor angle at point 1, Ra2 is the rotor angle at point 2, Ra3 is the rotor angle at point 3, Ra4 is the rotor angle at point 4, Rt1 is the rotor thickness at point 1, Rt2 is the rotor thickness at point 2, Rt3 is the rotor thickness at point 3 and Rt4 is the rotor thickness at point 4. The points are labelled according to Figure 7. The results reported in Figure 6 show less sensitivity to the first and second thickness points for both rotor and stator blades, and hence these are omitted, and the total number of decision variables is reduced to 11.

The search space is defined by setting the upper and lower limits of each decision variable as summarised in Table 2. The upper and lower limits are selected around the reference values based on manual iterations that aim at preserving a reasonable shape for the blade cross section.

The objective of this optimisation run is to maximise the total-to-total efficiency, whilst targeting the mass-flow rate defined by the cycle analysis. The target mass-flow rate for the $TiCl_4$, C_6F_6 and SO_2 cases are 1241, 877

and 781 kg/s, respectively, while the target tolerance is set to ±2%. The structural constraints for both rotor and stator blades are set to not exceed a stress limit of 400 MPa, calculated by dividing the yield strength of the working material at 650 ºC, which is around 1042 MPa [38], by a safety factor of 2.5.

The selected optimisation solver is genetic algorithm applied through ANSYS workbench and linked to the surrogate model. The initial population size and number of samples per iteration is 100. The convergence criteria are set to either achieving a stability percentage of 2% or reaching a maximum number of iterations of 50. Once the optimisation run is complete, five candidate points are calculated and verified against the physical model. The deviation between the physical model and response surface optimisation results are then assessed to check the accuracy of the surrogate model. If the measured deviations are high, the response surface is further refined using the candidate points and the optimisation process is repeated. Among the five candidate points, the design showing the best performance, as well as a good agreement with the verified results is selected.

3 CFD/FEA MODEL VERIFICATION

Due to the fact that supercritical carbon dioxide is a recent technology and the experimental work in the literature is limited to small-scale radial turbomachines there is no suitable data against which to validate the current CFD/FEA model for sCO_2 applications. However, the aerodynamic and structural solvers used in this study have been widely deployed in the analysis of other large-scale turbines, for example [31, 32]. A numerical model analysing the conjugate aerodynamic-structural interaction of a 15 MW sCO_2 single-stage axial turbine is selected to verify the physical CFD/FEA model presented in this paper [7]. The case definition and the operating conditions are presented in Table 3.

A comparison of the main performance metrics as well as the structural simulation are summarised in Table 4. A good agreement is observed between the two models in terms of mass-flow rate, total-to-static efficiency, and maximum von mises stress with deviations of 4.5%, 0.2%, and 1.7%, respectively. However, larger deviations are observed for the power output and degree of reaction. This could be the result of an inaccurate replication of the geometry due to uncertainties in extracting precise shape data from published figures rather than explicit tables; although, the main geometric parameters like hub/shroud diameters, inlet/outlet blade angles, inlet/outlet fillet radii, stagger angle, and chord size are identical.

4 RESULTS AND DISCUSSION

The blade shape of the three proposed working fluids is optimised and compared to the reference geometry created using preliminary mean-line design tool for the first stage of each turbine design. The performance of the optimised blades is further investigated by calculating the loss breakdown structure and comparing the results to the reference geometries to realise how the optimisation process has controlled the performance and enhanced the total-to-total efficiency. The computer used to run these cases contains a 3GHz processor with 36 cores, 48 MB cash memory, 128 GB of RAM and 2 TB SSD hard drive.

4.1 Optimised blades using different blends

Numerous design points are created using the high fidelity CFD/FEA model to create a response surface where 151 model are created using the design of experiments algorithm and an additional 250 design points are created by the response surface solver as refinement points to improve the accuracy of the surrogate model. For each design point, 11 geometric parameters are defined as inputs while the main objectives and constraints are evaluated to form the learning points to the surrogate model. Verification points are introduced to evaluate the performance of the surrogate model and its uncertainty. The uncertainty of the optimised candidate design points is found to be less than 0.3% for the total-to-total efficiency and 1% for the mass-flow rate, stator maximum stress and rotor maximum stress in all the proposed cases.

The response for different working fluids following the prespecified ranges of decision variables are evaluated and the results ranges are recorded in Table 5 where, η_{tt} is the total-to-total efficiency percentage, $\dot{m}$ is the mass-flow rate in kg/s, σ_S is the stator maximum equivalent stress in MPa and σ_R is the rotor maximum equivalent stress in MPa. These results include the size of the search space covered within this study. It can be noted that changes to the blade profile can lead to significant deviations in key parameters like mass-flow rate and stress levels, as well as the total-to-total efficiency. The sensitivity of the output parameters to the inputs is evaluated and further discussed in section 4.4, which can inform the elimination of less important input variables to reduce computational power and decrease uncertainty of the surrogate model. This can be expected to speed up when the design process when applied to all the stages of the final SCARABEUS turbine.

The optimised blades for different sCO_2 blends are introduced in Figure 8 and compared to the reference geometries for both the rotor and stator blades. The optimised blade geometry of the 1st stage of the sCO_2-SO_2 case study is shown by Figure 8 (a) where it can be seen that the stator blade curvature is relaxed near the TE to decrease

the stator outlet angle. Subsequently, the rotor leading edge angle is decreased in response to the changes made to the stator, and decreased near the training edge, while the TE thickness is decreased by almost 60% to decrease TE losses. These changes improve the aerodynamic performance by decreasing the deviation angle between the flow stream and the blade.

By investigating the optimised blade geometry of the sCO_2-C_6F_6 case study (Figure 8 (b)), similar trends to the SO_2 blades are observed where the stator angle distribution near the trailing edge is decreased while the thickness of the stator blade near the trailing edge is increased. The rotor thickness is decreased near the second half and at the TE while the angle distribution along the rotor chord line has been slightly modified by decreasing the angle values of the first half of the aerofoil and increasing the values of the second half. The optimised blade geometry of the sCO_2-$TiCl_4$ case study (Figure 8 (c)) agrees with the other two blends in decreasing the rotor outlet angle and decreasing the trailing edge thickness of both rotor and stator; however, the first part of the rotor blade angle is significantly decreased.

A comparison of the reference and optimised blade thickness and angle distributions is provided for each blend in Figure 9. The results correspond to the changes reported in Figure 8 and provides the optimised distributions explicitly. The performance improvement for the three proposed working fluids are reported in Table 6. It could be seen from the table that the optimisation has succeeded in increasing the total-to-total efficiency for the three blends, whilst achieving a design with a feasible mass-flow rate, as prescribed by the cycle requirements and that ensures safe operating with a peak equivalent stress less than 400 MPa. It should be noted that the reference values mentioned in the table are calculated using the physical model, and report some deviations compared to the mean-line design model. Some deviations between the MLD and CFD model results are expected due to the inherent simplicity of the mean-line approach, and the limitations of the mean-line model in evaluating aerodynamic losses by using loss correlations developed for traditional working fluids. However, these have been investigated and quantified by the authors [30]. Absolute efficiency increase of 2.54 pp, 2.06 pp, and 1.76 pp is achieved for the sCO_2-SO_2, sCO_2-C_6F_6, and sCO_2-$TiCl_4$ designs, respectively. By comparing achieved efficiencies for the different blends, it can be seen that the highest efficiency is obtained for the $TiCl_4$ design which is 0.12 pp larger than the C_6F_6 design and 0.13 pp larger than the SO_2 design, while the efficiencies obtained for the C_6F_6 and SO_2 designs are almost the same.

The mass-flow rate decreased in all the designs to bring the design within the feasible range of operation defined by ±2% of the designed mass-flow rate mentioned in

List of tables

Table 1 because the mean-line design has been found to underestimate the mass-flow rate of the reference design point. The reduction in mass-flow rate is reflected by a reduction in power output although the efficiency is increased. The results in Table 6 show that the best performance is obtained for the three blends at a slightly larger degree of reaction, typically around 0.63, compared to the value of 0.5 assumed during the preliminary calculations. The flow coefficient is very close to the preliminary design value of 0.5 and the loading coefficient is nearly 10% larger than the preliminary design value. For the stress limits, the reference design points of the SO_2 stator and the $TiCl_4$ stator are unsafe with maximum stress values over the limit of 400 MPa; however, the optimised design points succeed at maintaining peak stresses under the limits for all the design case studies.

To further understand the differences between the blade shapes of the three blends, the optimised aerofoils are reported in Figure 10. It is expected that the differences between the three cases are not only due to the differences in properties, but also due to the different boundary conditions generated from the thermodynamic cycle optimisation for each three blends. Thus, the influence of these effects on the resulting blade shape and aerodynamic performance is combined and they cannot be easily separated. However, it can be clearly noted the larger chord size of the $TiCl_4$ case, which results from the higher stresses that are estimated during the preliminary mean-line design phase which drives the design to a lower number of blades per stage. Subsequently, the pitch and chord size are both increased to maintain a fixed pitch to chord ratio. The similarity between SO_2 and C_6F_6 designs reflects the similarity of the properties of the mixtures, the cycles layout, and the boundary conditions reported in

List of tables

Table 1. The blade shape differences can also be linked to the mixtures properties by comparing the hydraulic properties of the three mixtures reported in Table 7. It can also be seen that the blade thickness is higher near the leading edge for the $TiCl_4$ case, followed by C_6F_6 and SO_2, reflecting the density variations as the higher the density, the lower the flow path cross section and the thicker the blade. The difference between inlet and outlet blade angles reflects the variation in the dynamic viscosity to reduce secondary flows, where the higher the viscosity the lower the difference in the blade angles. This is clear from Figure 10, as the highest blade angle variation appears in the SO_2 case followed by the C_6F_6 and $TiCl_4$ cases.

4.2 Loss breakdown analysis

The performance of the proposed designs is further investigated by analysing the aerodynamic loss structure of the reference and optimised geometries to compare the weight of different sources of loss. The expected aerodynamic losses of a subsonic axial turbine stage running at the design operating conditions are the endwall losses, profile losses, trailing edge losses and tip clearance losses [39]. An overview of the loss structure is shown by Figure 11 where the entropy distribution along the axial direction from inlet to outlet is presented. The stator domain is represented along the axial direction from 0 to 1, while the rotor domain is represented between 1 and 2. The calculated entropy values are mass flow averaged quantities evaluated at different axial locations along the streamwise direction. The dominating loss regions can be directly identified from the figure given the axial locations of the stator/rotor blades, inlet/outlet domains and the stator/rotor axial gap.

The reference cases lead to a larger entropy increase at the stage outlet in all the designs reflecting the achieved performance improvement by optimising the blade geometries for the three proposed blends. The curves for the SO_2 and C_6F_6 designs are close to each other while the $TiCl_4$ design reports less entropy generation with higher total-to-total efficiency. This is in agreement with the efficiency results mentioned in Table 6. A significant reduction in entropy generation in both the rotor and stator blades can be observed in the figure and can be further clarified by carrying out a loss audit of the reference and optimised designs.

The loss breakdown is obtained following the approach described by De Servi et al. [25] where the sources of loss are evaluated by setting up three CFD models for each design point according to the structure mentioned by Table 8. The difference between the entropy generation from model one and two accounts for the tip leakage loss while the total entropy rise in the second model is due to end wall, profile and TE losses in the rotor and stator. To

quantify each source individually, the third model eliminates end wall effects by setting free slip boundary conditions near the end walls so that the remaining losses are profile and trailing edge losses. The difference between entropy from inlet to a plane at the trailing edge accounts for the profile losses while the difference between the plane at the trailing edge and the outlet plane is due to the trailing edge losses. By subtracting the values obtained from model two and model three, endwall losses can be evaluated.

A complete loss breakdown structure of the reference and optimised blades for the three blends are summarised in Figure 12 where the losses due to stator endwall (SEW), stator profile (SPF), stator trailing edge (STE), rotor endwall (REW), rotor profile (RPF), rotor trailing edge (RTE), and tip clearance (TC) are presented. The reference points show a high entropy increase relative to the optimised blades for all the working fluids with the highest value for the SO_2 design followed by C_6F_6 and the $TiCl_4$, respectively. By looking at the SO_2 design it could be seen that both stator and rotor loss components are reduced with a dominant reduction in the stator endwall, stator trailing edge, and rotor endwall losses. Similar findings are recorded for the C_6F_6 design, however the reduction in the tip clearance is substantial. For the $TiCl_4$ design, tip clearance losses are increased, but with a reduction to stator endwall, stator profile, stator trailing edge, rotor endwall, and rotor trailing edge losses.

The differences between reference and optimised loss breakdown components for the three blends have shown that the blade profile generated using the mean-line design is not ideal and generates large secondary flows and vortices compared to the optimised profiles as noted from the reduction in secondary flows and profile losses. The trailing edge losses also show a reduction in both the stator and rotor blades indicating an over estimation of TE thickness blades within the mean-line design model; however, TE losses are not overly dominant. The tip clearance show minor changes due to design optimisation which means that it cannot be improved using profile modifications; this is expected as TC losses are mainly due to the tip gap thickness and the stage pressure ratio [40].

The contribution of each source of loss to the total aerodynamic performance is summarised in Table 9 where it is observed that the largest portion is due to tip leakage and the smallest potion is due to trailing edge loss. The endwall and profile losses are similar in most of the designs, although the endwall losses are higher that the profile losses in the reference design point. However, the optimised designs show less endwall losses indicating that the endwall losses are more affected by the optimisation process.

4.3 Sensitivity of output components

The number of decision variables needed to represent a single blade profile is relatively large, and this does not account for the blade shape radial variation which could imply increasing the number of decision variables by a factor of two or three times to obtain a full representation of a single blade. Thus, to make the optimisation process more effective and accurate, particularly considering extension to multiple stages, the number of decision variables should be limited to the most dominant variables. To this end, a sensitivity analysis has been performed to assess the importance of each input variable so that dominating parameters are established. The sensitivity of the output objectives and constraints to the eleven input variables used in this study is given by Figure 13. The sensitivity of total-to-total efficiency is shown by Figure 13 (a) where the most dominating parameters are the stator and rotor blade angles near the trailing edge. at the second mid-point on the angle distribution curve (point 3), as well as the outlet angles. Less dominant parameters affecting the efficiency, but non-negligible are the thickness points at the second half of the aerofoil near the trailing edge (point 3, 4). The other parameters also affect the efficiency; however, these are not significant. This indicates that the selected decision variables in this study are of reasonable importance, as anticipated during the initial selection process of variables. The local sensitivity of the mass- flow rate is shown by Figure 13 (b) where the dominating variables are mainly the angles of the second part of the aerofoil (points 3,4). The stator and rotor blade angles at points 3 and 4 are also found to be important in determining the stator and rotor peak stresses. In addition, the local sensitivity of stator peak stress shown by Figure 13 (c) are affected by the thickness distribution parameters of the stator (St3 and St4) while the rotor peak stress shown by Figure 13 (d) are affected by the thickness distribution parameters of the rotor (Rt3 and Rt4).

5 CONCLUSION

The blade shape optimisation of three turbine designs operating with CO_2 blended with $TiCl_4$, C_6F_6 or SO_2 has been presented. Comparing the reference and optimised blade geometries has revealed guidelines towards improving the efficiency of the stage by reducing aerodynamic losses. The common adjustments are decreasing stator and rotor trailing edge thickness, increasing stator thickness near the trailing edge, decreasing rotor thickness near the trailing edge and decrease the rotor outlet angle.

The accuracy of the surrogate model has been improved by defining a number of refinement points alongside the initial learning points created using the design of experiments to improve the model accuracy. The optimised

designs generated using the surrogate model have shown a deviation from the physical model in total-to-total efficiency of less than 0.3%, and a deviation in mass-flow rate and peak stresses less than 1% in all the design cases.

The optimisation results have shown an improvement to the aerodynamic performance of the three designs with efficiency increases of 2.54 pp, 2.06 pp, and 1.76 pp for the sCO_2-SO_2, sCO_2-C_6F_6, and sCO_2-$TiCl_4$ designs respectively, while the mass-flow rate is kept within 2% of the design value and peak stresses are limited to 400 MPa. The results have shown that the optimised blades are achieved at a degree of reaction, flow coefficient and loading coefficient around 0.63, 0.52 and 1.1, respectively, compared to design values of 0.5, 0.5 and 1.0 respectively. Assessing the loss breakdown reveals that the improved performance is mainly due to minimising the endwall and profile losses for both the rotor and stator blades. However, the reduction in endwall losses is the most dominant.

Additionally, a sensitivity analysis has revealed that the design variables with the most significant impact on the total-to-total efficiency are the stator and rotor blade angles within the second part of the aerofoil, which have also showed a significant effect on the mass-flow rate and peak stresses. The aerofoil thickness near the trailing edge of the stator and the rotor dominate the stator and rotor peak stresses, respectively.

Ultimately, the results from this study have shown the validity of the approach taken by the authors in designing this type of turbine with novel working fluids, for which the available loss models are not tested or calibrated. In addition, it is found that the sensitivity of the aerodynamic and structural performance parameters to the blade thickness at and near the leading edge of both rotor and stator blades is low, and hence variables controlling these aspects could be omitted in future studies. The number of decision variables applied using the proposed methodology is recommended to be kept less than 11 in order for the surrogate model to accurately represent the physical CFD/FEA model, without requiring excessing computational power.

FUNDING

This work was supported by the European Union's Horizon 2020 research and innovation programme under grant agreement No. 814985.

6 REFERENCES

[1] Crespi, F., Sánchez, D., Martínez, G. S., Sánchez-Lencero, T. and Jiménez-Espadafor, F., "Potential of supercritical carbon dioxide power cycles to reduce the levelised cost of electricity of contemporary concentrated solar power plants," *Applied Sciences* Vol. 10 No. 15 (2020): pp. 5049.

[2] Crespi, F., Rodríguez De Arriba, P., Sánchez, D., Muñoz, A. and Sánchez, T., "The Potential of Supercritical Cycles Based on CO2 Mixtures in Concentrated Solar Power Plants: An Exergy-Based Analysis," *Proceedings of the 6th International Seminar on ORC Power Systems, Munich, Germany*, Virtual, Online, 11-13 October, 2021, pp. 11-13.

[3] White, M. T., Bianchi, G., Chai, L., Tassou, S. A. and Sayma, A. I., "Review of supercritical CO_2 technologies and systems for power generation," *Applied Thermal Engineering* Vol. 185 (2021): pp. 116447.

[4] Crespi, F., De Arriba, P. R., Sánchez, D., Ayub, A., Di Marcoberardino, G., Invernizzi, C. M., Martínez, G., Iora, P., Di Bona, D. and Binotti, M. J. E., "Thermal efficiency gains enabled by using CO_2 mixtures in supercritical power cycles," *Energy* Vol. 238 (2022): pp. 121899.

[5] Morosini, E., Ayub, A., Di Marcoberardino, G., Invernizzi, C. M., Iora, P., Manzolini, G. J. E. C. and Management, "Adoption of the CO_2+ SO_2 mixture as working fluid for transcritical cycles: A thermodynamic assessment with optimized equation of state," *Energy Conversion and Management* Vol. 255 (2022): pp. 115263.

[6] Cho, J., Choi, M., Baik, Y. J., Lee, G., Ra, H. S., Kim, B. and Kim, M., "Development of the turbomachinery for the supercritical carbon dioxide power cycle," *International Journal of Energy Research* Vol. 40 No. 5 (2016): pp. 587-599.

[7] Zhang, H., Zhao, H., Deng, Q. and Feng, Z., "Aerothermodynamic design and numerical investigation of supercritical carbon dioxide turbine," *Turbo Expo: Power for Land, Sea, and Air*, Montreal, Canada, June 15-19, 2015, Vol. 56802, pp. V009T036A007.

[8] Crespi, F., Martínez, G., Rodriguez De Arriba, P., Sánchez, D. and Jiménez-Espadafor, F., "Influence of Working Fluid Composition on the Optimum Characteristics of Blended Supercritical Carbon Dioxide Cycles," *Turbo Expo: Power for Land, Sea, and Air*, Virtual, Online, 7-11 Jue, 2021, Vol. 85048, pp. V010T030A030.

[9] Aqel, O., White, M. and Sayma, A. "Binary interaction parameter uncertainty in the optimisation of a transcritical cycle: consequences on cycle and turbine design." Virtual online.

[10] Brun, K., Friedman, P. and Dennis, R. Fundamentals and applications of supercritical carbon dioxide (sCO_2) based power cycles. Woodhead publishing (2017).

[11] Sathish, S., Kumar, P., Namburi, A. N., Swami, L., Fuetterer, C. and Gopi, P. C., "Novel Approaches for sCO_2 Axial Turbine Design," *Turbo Expo: Power for Land, Sea, and Air*, Phoenix, Arizona, USA, 17-21 June, 2019, Vol. 58721, pp. V009T038A011.

[12] Maral, H., Alpman, E., Kavurmacıoğlu, L. and Camci, C., "A genetic algorithm based aerothermal optimization of tip carving for an axial turbine blade," *International Journal of Heat and Mass Transfer* Vol. 143 (2019): pp. 118419.

[13] Berchiolli, M., Guarda, G., Walsh, G. and Pesyridis, A., "Turbocharger Axial Turbines for High Transient Response, Part 2: Genetic Algorithm Development for Axial Turbine Optimisation," *Applied Sciences* Vol. 9 No. 13 (2019): pp. 2679.

[14] Klonowicz, P., Lampart, P., Suchocki, T., Zaniewski, D. and Klimaszewski, P., "Optimization of an axial turbine for a small scale ORC waste heat recovery system," *Energy* Vol. 205 (2020): pp. 118059.

[15] Persico, G., Romei, A., Dossena, V. and Gaetani, P., "Impact of shape-optimization on the unsteady aerodynamics and performance of a centrifugal turbine for ORC applications," *Energy* Vol. 165 (2018): pp. 2-11.

[16] Ennil, A. B., Al-Dadah, R., Mahmoud, S., Rahbar, K. and Aljubori, A., "Minimization of loss in small scale axial air turbine using CFD modeling and evolutionary algorithm optimization," *Applied Thermal Engineering* Vol. 102 (2016): pp. 841-848.

[17] Asgarshamsi, A., Benisi, A. H., Assempour, A. and Pourfarzaneh, H., "Multi-objective optimization of lean and sweep angles for stator and rotor blades of an axial turbine," *Proceedings of the Institution of Mechanical Engineers, Part G: Journal of aerospace engineering* Vol. 229 No. 5 (2015): pp. 906-916.

[18] Noori Rahim Abadi, S. M. A., Ahmadpour, A., Abadi, S. M. N. R. and Meyer, J. P., "CFD-based shape optimization of steam turbine blade cascade in transonic two phase flows," *Applied Thermal Engineering* Vol. 112 (2017): pp. 1575-1589.

[19] Kawatsu, K., Tani, N., Shimagaki, M., Uchiumi, M., Yamanishi, N., Mitsuhashi, K. and Mizuno, T., "Multi objective optimization of a supersonic axial turbine blade row shape for rocket engine turbopump," *47th AIAA/ASME/SAE/ASEE Joint Propulsion Conference & Exhibit*, San Diego, California, 31 July 2011 - 03 August 2011, pp. 5784.

[20] Cho, S.-Y., Yoon, E.-S. and Choi, B.-S., "A Study on an axial-type 2-D turbine blade shape for reducing the blade profile loss," *KSME International Journal* Vol. 16 No. 8 (2002): pp. 1154-1164.

[21] Pakatchian, M. R., Saeidi, H. and Ziamolki, A., "CFD-based blade shape optimization of MGT-70 (3) axial flow compressor," *International Journal of Numerical Methods for Heat & Fluid Flow* (2019).

[22] Sivashanmugam, V. K., Arabnia, M. and Ghaly, W., "Aero-structural optimization of an axial turbine stage in three-dimensional flow," *Turbo Expo: Power for Land, Sea, and Air*, Glasgow, UK, June 14–18, 2010, Vol. 44021, pp. 967-980.

[23] Schwerdt, L., Hauptmann, T., Kunin, A., Seume, J. R., Wallaschek, J., Wriggers, P., Panning-Von Scheidt, L. and Löhnert, S., "Aerodynamical and structural analysis of operationally used turbine blades," *Procedia CIRP* Vol. 59 (2017): pp. 77-82.

[24] Yoon, S., Vandeputte, T., Mistry, H., Ong, J. and Stein, A., "Loss audit of a turbine stage," *Journal of Turbomachinery* Vol. 138 No. 5 (2016): pp. 051004.

[25] De Servi, C. M., Burigana, M., Pini, M. and Colonna, P., "Design method and performance prediction for radial-inflow turbines of high-temperature mini-Organic Rankine Cycle power systems," *Journal of Engineering for Gas Turbines and Power* Vol. 141 No. 9 (2019).

[26] Keep, J. A. and Jahn, I. H., "Numerical loss investigation of a small scale, low specific speed supercritical CO_2 radial inflow turbine," *Journal of Engineering for Gas Turbines and Power* Vol. 141 No. 9 (2019).

[27] Salah, S. I., Khader, M. A., White, M. T. and Sayma, A. I., "Mean-Line Design of a Supercritical CO_2 Micro Axial Turbine," *Applied Sciences* Vol. 10 No. 15 (2020): pp. 5069.

[28] Binotti, M., Marcoberardino, G. D., Iora, P., Invernizzi, C. and Manzolini, G., "SCARABEUS: Supercritical carbon dioxide/alternative fluid blends for efficiency upgrade of solar power plants," *AIP Conference Proceedings,* Vol. 2303, pp. 130002.

[29] Aungier, R. H., "Turbine aerodynamics," *ASME, New York* (2006).

[30] Abdeldayem, A., White, M. T. and Sayma, A. I., "Comparison of CFD Predictions of Supercritical Carbon Dioxide Axial Flow Turbines Using a Number of Turbulence Models," *Turbo Expo: Power for Land, Sea, and Air*, Virtual, Online, June 7–11, 2021, Vol. 85048, pp. V010T030A010.

[31] Jang, H. J., Kang, S. Y., Lee, J. J., Kim, T. S. and Park, S. J., "Performance analysis of a multi-stage ultra-supercritical steam turbine using computational fluid dynamics," *Applied Thermal Engineering* Vol. 87 (2015): pp. 352-361.

[32] Touil, K. and Ghenaiet, A., "Simulation and analysis of vane-blade interaction in a two-stage high-pressure axial turbine," *Energy* Vol. 172 (2019): pp. 1291-1311.

[33] Dubiez-Le Goff, S., Couturier, R., Guétaz, L. and Burlet, H., "Effect of the microstructure on the creep behavior of PM Udimet 720 superalloy—experiments and modeling," *Materials Science and Engineering: A* Vol. 387 (2004): pp. 599-603.

[34] Hatami, M., Cuijpers, M. C. and Boot, M. D., "Experimental optimization of the vanes geometry for a variable geometry turbocharger (VGT) using a Design of Experiment (DoE) approach," *Energy Conversion and Management* Vol. 106 (2015): pp. 1057-1070.

[35] Toft, H. S., Svenningsen, L., Moser, W., Sørensen, J. D. and Thøgersen, M. L., "Assessment of wind turbine structural integrity using response surface methodology," *Engineering Structures* Vol. 106 (2016): pp. 471-483.

[36] Wang, S., Jian, G., Xiao, J., Wen, J. and Zhang, Z., "Optimization investigation on configuration parameters of spiral-wound heat exchanger using Genetic Aggregation response surface and Multi-Objective Genetic Algorithm," *Applied Thermal Engineering* Vol. 119 (2017): pp. 603-609.

[37] Viana, F. A., Haftka, R. T. and Steffen, V., "Multiple surrogates: how cross-validation errors can help us to obtain the best predictor," *Structural and Multidisciplinary Optimization* Vol. 39 No. 4 (2009): pp. 439-457.

[38] Screrzenie, F. and Maurer, G., "Development of Udimet720 for high strength disk application," *Proceedings of Superalloys* (1984).

[39] Denton, J. D. *Loss mechanisms in turbomachines*. American Society of Mechanical Engineers (1993).

[40] Xiao, X., Mccarter, A. A. and Lakshminarayana, B., "Tip clearance effects in a turbine rotor: part I—pressure field and loss," *J. Turbomach.* Vol. 123 No. 2 (2001): pp. 296-304.

LIST OF TABLES

TABLE 1 DESIGN CONDITIONS FOR THE THREE CO_2 BLENDS

Working fluid	-	sCO2-SO2	sCO2-C6F6	sCO2-TiCl4
Blend molar fraction	%	30	14.5	17
Inlet total pressure	bar	238.9	238.9	242.6
Inlet total temperature	K	973.15	973.15	973.15
Turbine outlet s. pressure	bar	68.3	59.1	95.5
Mass flow rate	kg/s	780.84	877.3	1241.2
Stage 1outlet s. pressure	bar	207.5	199.5	200.1
Stage actual enthalpy drop	kJ/kg	18.8	18.8	18.8
Hub radius	mm	420	420	420
Rotational speed	RPM	3000	3000	3000
Number of stages	-	9	8	5

TABLE 2 DECISION VARIABLES

Parameter	Unit	Value		
		Reference	Min	Max
St3	mm	5.7	4	7
St4	mm	0.7	0.2	1
Sa2	deg	5	-5	15
Sa3	deg	45	35	55
Sa4	deg	66.3	55	80
Rt3	mm	5.6	4	7
Rt4	mm	0.7	0.2	1
Ra1	deg	0	-10	10
Ra2	deg	-5	-15	5
Ra3	deg	-45	-55	-35
Ra4	deg	-64.93	-75	-55

TABLE 3 DEFINITION OF THE VERIFICATION CASE STUDY

Parameter	Unit	Value
Turbine inlet pressure	bar	130
Turbine inlet temperature	K	773
Turbine outlet pressure	bar	80
Mean blade diameter	mm	389
Rotational speed	RPM	10000
Mass flowrate	kg/s	250

TABLE 4 RESULTS OF THE VERIFICATION CASE STUDY

Parameter	Unit	Ref. [7]	Numerical model	Deviation (%)
Mass flow rate	kg/s	250	238.81	-4.5%
Power	MW	15	13.75	-8.3%
Degree of reaction	-	0.28	0.3	7.1%
Flow coefficient	-	0.55	0.569	3.5%
Total to static efficiency	%	83.96	83.782	-0.2%
Rotor Max. deflection	mm	0.061	0.056	-8.2%
Rotor Max. Von Mises stress	MPa	646.8	636	-1.7%

TABLE 5 CALCULATED RANGES OF OUTPUT PARAMETERS

	SO_2		C_6F_6		$TiCl_4$	
	Min.	Max.	Min.	Max.	Min.	Max.
$\boldsymbol{\eta_{tt}}$	69.8	93.9	60.5	93.7	76.5	94.8
$\boldsymbol{\dot{m}}$	270.1	1449.6	385	1520	238	2182
$\boldsymbol{\sigma_S}$	60	1380	90	827	69.6	3608
$\boldsymbol{\sigma_R}$	45.2	490	57	563	36	728

TABLE 6 RESULTS OF OPTIMISING BLADE SHAPES

Parameter	Unit	SO_2 Ref.	SO_2 Opt.	C_6F_6 Ref.	C_6F_6 Opt.	$TiCl_4$ Ref.	$TiCl_4$ Opt.
Total-to-total efficiency	%	88.82	91.36	89.31	91.37	89.69	91.45
Mass flow rate	kg/s	814.4	790.65	989.4	879.1	1426.3	1252.5
Power	MW	15.05	14.69	18.24	16.59	25.35	23.54
Degree of reaction	-	0.32	0.65	0.44	0.62	0.45	0.62
Flow coefficient	-	0.51	0.53	0.56	0.51	0.56	0.53
Loading coefficient	-	0.89	1.12	0.91	1.09	0.86	1.14
Stator Max. stress	MPa	447.42	347.42	393.30	346.55	509.12	401.44
Rotor Max. stress	MPa	188.76	246.67	210.98	244.00	250.67	392.06

TABLE 7 PROPERTIES OF THE THREE MIXTURES AT THE INLET CONDITIONS

	SO_2	C_6F_6	$TiCl_4$
Molar fraction (%)	30	14.5	17
Density (ρ) (kg/m^3)	146.6	185.4	200.5
Dynamic Viscosity (μ) ($Pa.s$)	4.70E-05	5.05E-05	5.11E-05

TABLE 8 LOSS BREAKDOWN APPROACH BY DE SERVI ET AL.

Model	Description
Model 1: Standard model	Total entropy increase (Inlet to Outlet)
Model 2: No tip clearance	Entropy increase across stator and rotor individually from inlet to outlet
Model 3: No tip clearance / Endwall	Entropy increase from Inlet to location at the trailing edge and from trailing edge to outlet for stator and rotor blades

TABLE 9 RELATIVE LOSS BREAKDOWN BY COMPONENT

	SO_2 Ref.	SO_2 Opt.	C_6F_6 Ref.	C_6F_6 Opt.	$TiCl_4$ Ref.	$TiCl_4$ Opt.
Endwall	27.9%	22.2%	31.2%	20.5%	29.7%	17.6%
Profile	21.9%	23.8%	20.2%	23.9%	21.5%	20.1%
Trailing edge	15.4%	10.5%	13.5%	11.8%	13.7%	9.0%
Tip clearance	34.8%	43.5%	35.1%	43.8%	35.0%	53.3%

LIST OF FIGURES

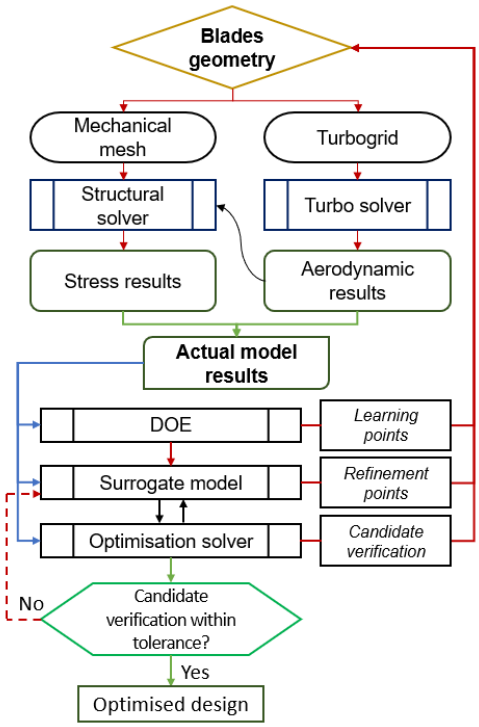

FIGURE 1 OVERVIEW OF THE OPTIMISATION MODEL

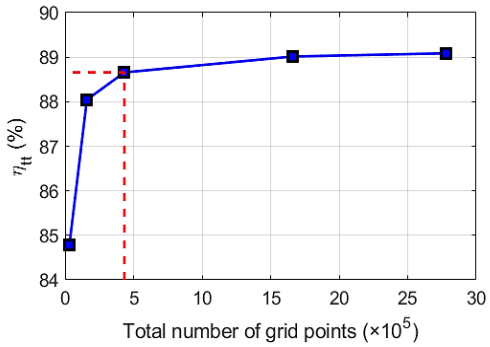

FIGURE 2 MESH INDEPENDENCE STUDY FOR THE C_6F_6 CASE

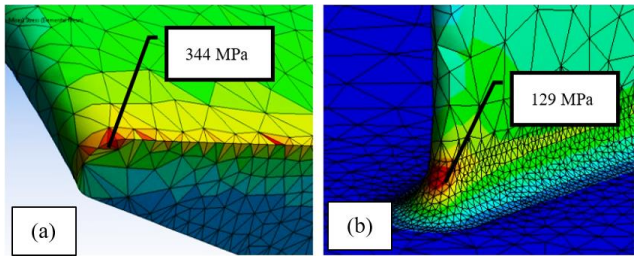

FIGURE 3 EFFECT OF BASE FILLET ON FEA RESULTS, (A) WITHOUT FILLET, (B) WITH FILLET.

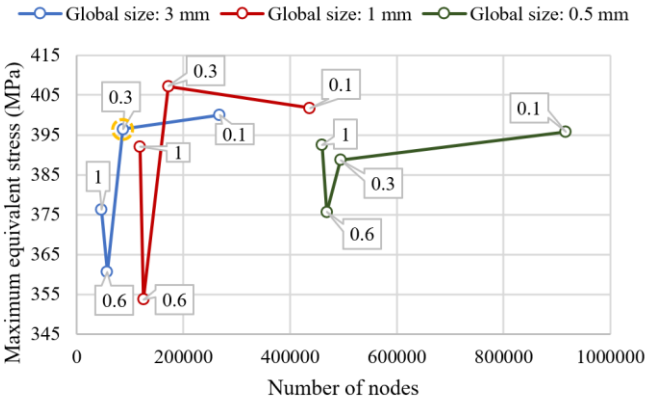

FIGURE 4 FEA MESH ANALYSIS OF THE SCO_2-C_6F_6 STATOR BLADE FOR DIFFERENT GLOBAL/LOCAL ELEMENT SIZES

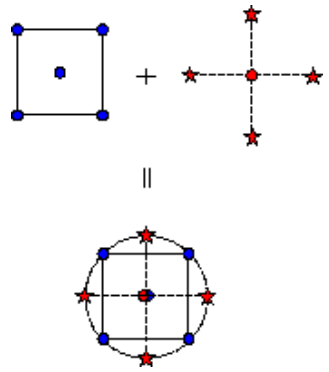

FIGURE 5 CENTRAL COMPOSITE DESIGN OF TWO DECISION VARIABLES

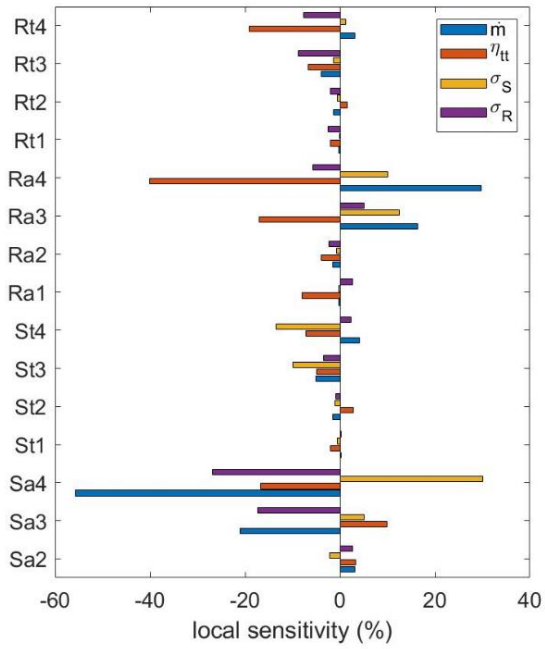

FIGURE 6 PRELIMINARY SENSTIVITY STUDY SOLVING 15 DECISION VARIABLES, SCO_2-SO_2 MODEL

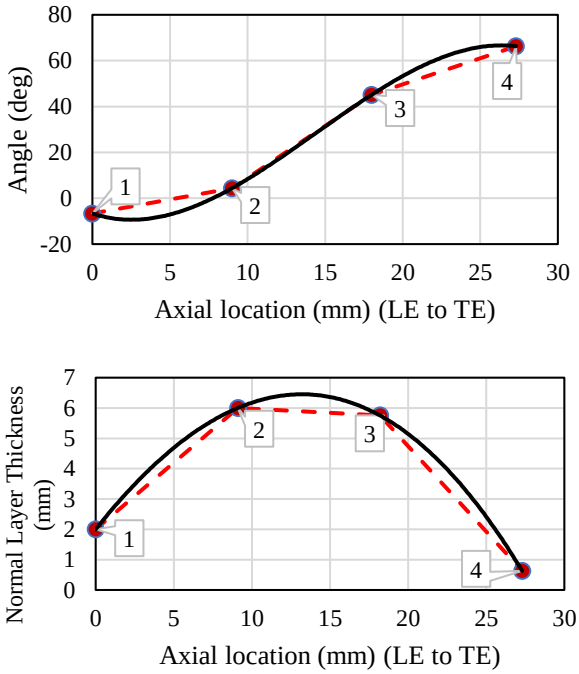

FIGURE 7 BLADE PROFILE REPRESENTATION USING ANGLE AND THICKNESS DISTRIBUTION

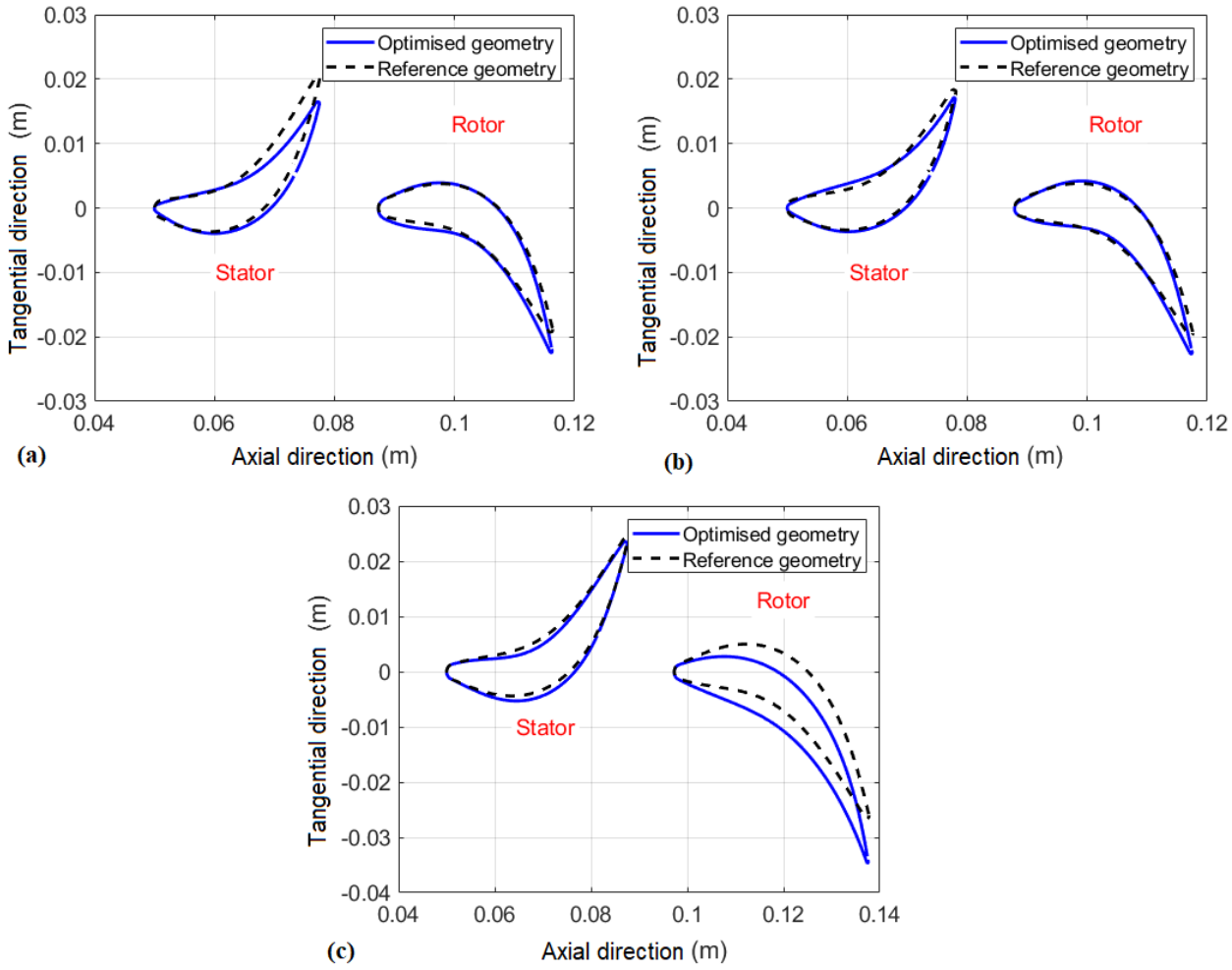

FIGURE 8 COMPARISON BETWEEN REFERENCE AND OPTIMISED BLADES OF THE 1ST STAGE FOR: (A) SCO_2-SO_2, (B) SCO_2-C_6F_6, AND (C) SCO_2-$TICL_4$

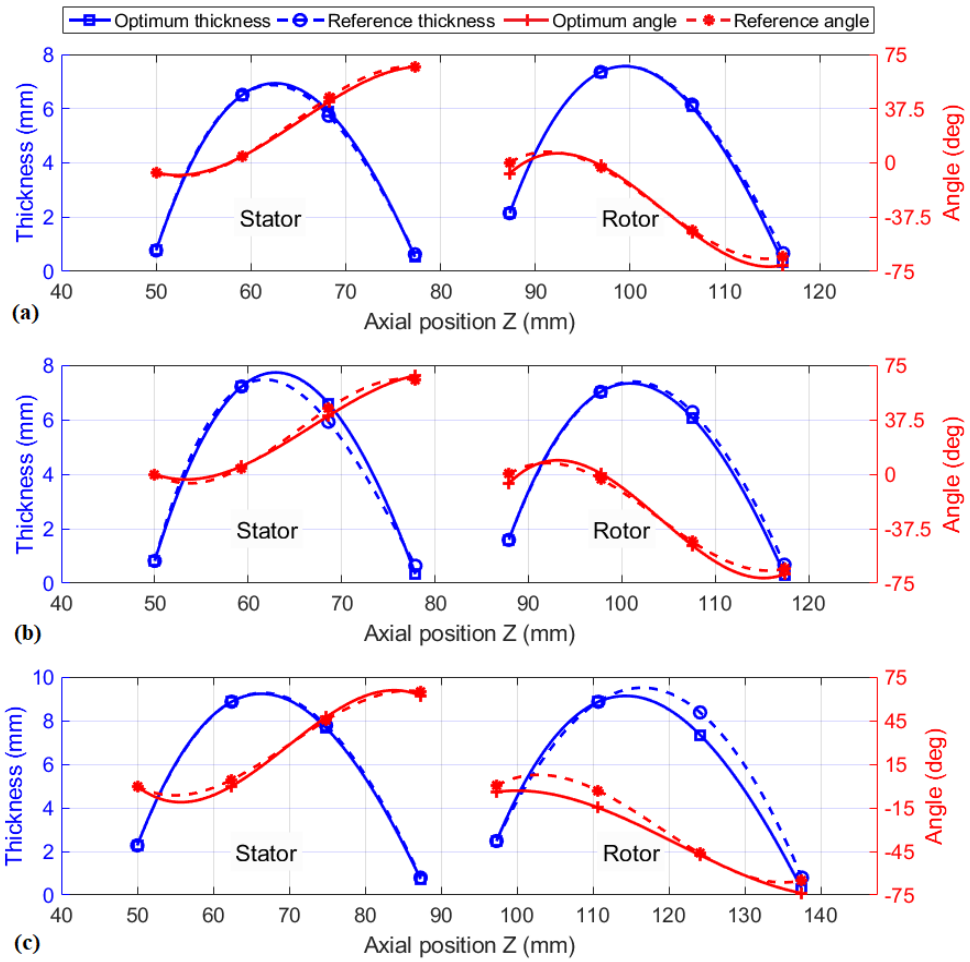

FIGURE 9 COMPARISON BETWEEN REFERENCE AND OPTIMISED BLADE THICKNESS/ANGLE DISTRIBUTION FOR DIFFERENT BLENDS. (A) SCO_2-SO_2, (B) SCO_2-C_6F_6, AND (C) SCO_2-$TICL_4$

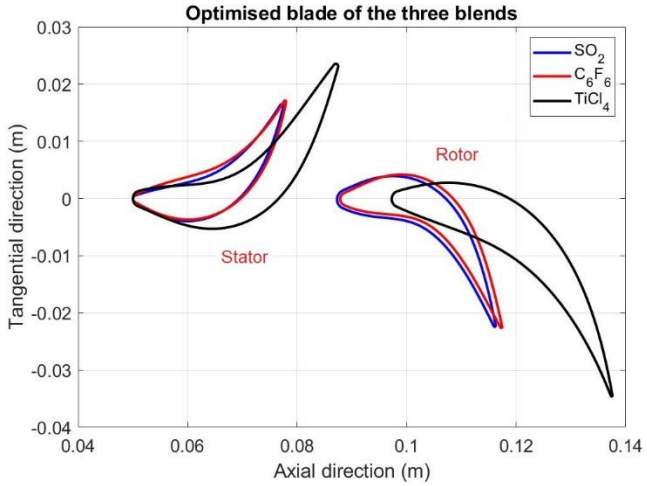

FIGURE 10 COMPARISON BETWEEN OPTIMISED BLADE SHAPES FOR THE THREE BLENDS

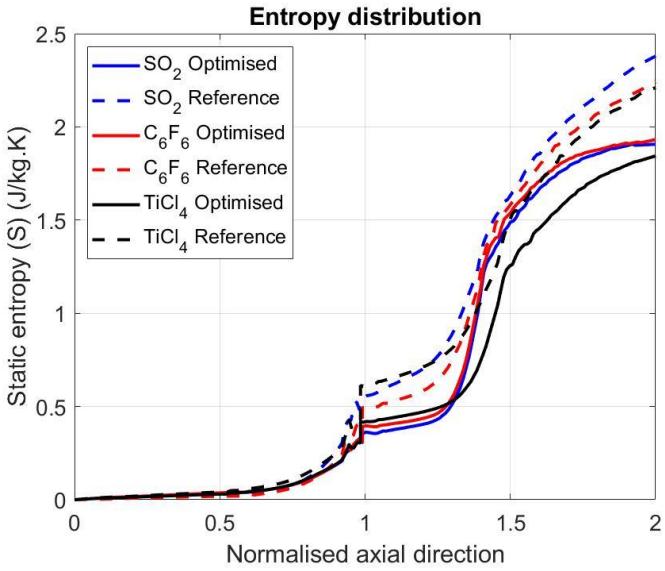

FIGURE 11 ENTROPY DISTRIBUTION ALONG THE NORMALISED AXIAL DIRECTION FOR THE 1ST STAGE FROM INLET TO OUTLET FOR DIFFERENT BLENDS

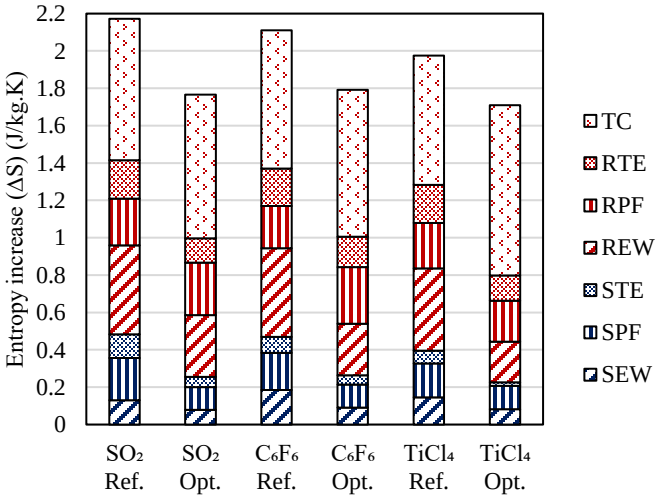

FIGURE 12 LOSS BREAKDOWN STRUCTURE FOR REFERENCE AND OPTIMISED GEOMETRIES

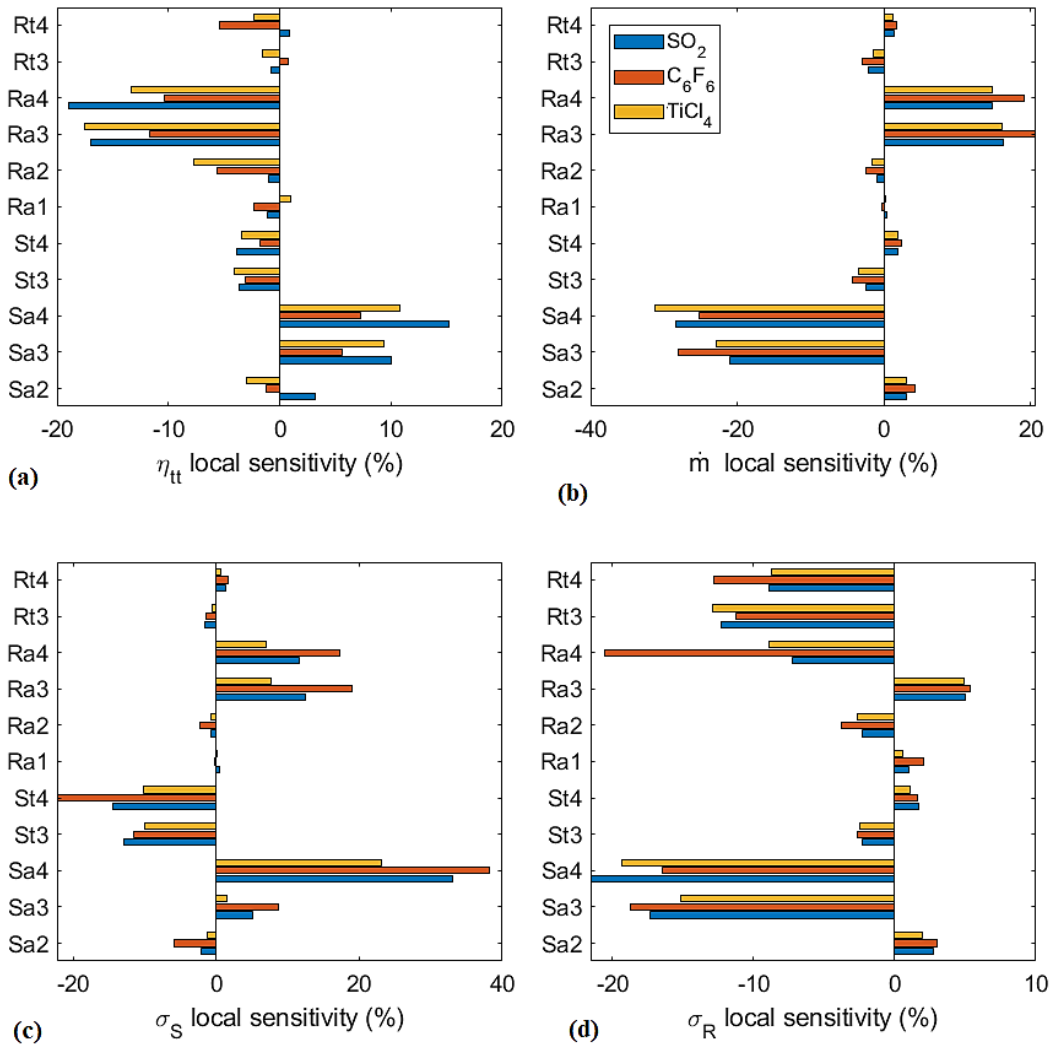

FIGURE 13 LOCAL SENSITIVITY OF OBJECTIVES AND CONSTRAINTS. (A) TOTAL-TO-TOTAL EFFICIENCY, (B) MASS FLOW RATE, (C) STATOR MAXIMUM EQUIVALENT STRESS, AND (D) ROTOR MAXIMUM EQUIVALENT STRESS